Ocean Engineering 195 (2020) 106729

Contents lists available at ScienceDirect

Ocean Engineering

journal homepage: www.elsevier.com/locate/oceaneng

Short communication

Chaotic motion of the parametrically excited roll motion for a class of ships in regular longitudinal waves

Liangqiang Zhou *, Fangqi Chen

Department of Mathematics, Nanjing University of Aeronautics and Astronautics, Nanjing, 210016, China

ARTICLE INFO

Keywords:
Ship capsizing
Chaos
Parametrically excited roll motion
Melnikov method

ABSTRACT

Employed both analytical and numerical methods, chaotic motions for the parametrically excited roll motion of a ship in regular longitudinal waves are investigated in this paper. It is presented that the mechanism for chaos is the intersection of the stable and unstable manifolds of the homoclinic orbits or heteroclinic cycle. The parameter conditions for chaos are obtained rigorously with the Melnikov method. The chaotic regions of the system parameters are illustrated. The chaotic feature on the system parameters is discussed in detail. It is obtained that the critical values of chaos for homoclinic orbits increase monotonously as the increasing of the nonlinear roll attenuation coefficient, while the critical values of chaos for the heteroclinic cycle decrease monotonously as the increasing of the nonlinear roll attenuation coefficient. On the other hand, critical values of chaos for both homoclinic orbits and heteroclinic cycle increase monotonously as the increasing of the excitation amplitude. It is also demonstrated that there exist chaotic bands for this model. Numerical simulations verify the analytical results.

1. Introduction

The navigation of ships in deep sea is a complicated dynamic process. Chaotic vibrations of ships may lead to capsize. Therefore, it is meaningful to study chaotic dynamics of ships. Recently, a lot of researchers have investigated chaotic motions of various ship models. Using an analytical and digital analog-computer simulation investigation, Nayfeh and Sanchez (1986) studied chaos and dynamic instability of the rolling motion for ships in beam, following, and head seas. Complicated rolling responses including jumps, period-multiplying bifurcations and chaos were presented. Employing a numerical, phenomenological approach, Virgin (1987) investigated the nonlinear rolling responses of a vessel including chaotic motions leading to capsize in regular seas. The stability of the periodic motion, and in particular the possibility of capsize were explored. By using the numerical time simulation, Kan and Taguchi studied chaos and fractal in capsizing phenomenon (Kan and Taguchi, 1990), in asymmetric capsizing equation (Kan and Taguchi, 1991), as well as in forced Mathieu type capsize equation (Kan and Taguchi, 1992) of a ship in quartering seas, respectively. A safe basin defined as a non-capsizing region in the phase plane of rolling angle and rolling velocity was obtained for the fixed control parameters such as forcing frequency, forcing amplitude and damping coefficient. Applying global analysis techniques, Falzarano et al. (1992) studied transient rolling motions of a small ship which is subjected to a periodic wave excitation. It was presented that the transition which this boundary makes from regular to fractal, implied a loss in predictability of the ship's eventual state. Using the path integral method, Liu and Tang (2013) investigated the random jumping of ship rolling excited by the narrow band waves. It was found that the ship rolling had two attraction regions when the effect of liquid on board was considered. Using a real-time online prediction method, Liu and Yang (2011) studied the chaotic characteristics of ship rolling motion. Based on the chaos system reconstruction method and G–P method, Li et al. (2016) investigated prediction of ship motions. Using Lyapunov characteristic exponents, Hu et al. (2010) investigated chaotic roll motions of ships in regular longitudinal waves. The safe and unsafe regions of target ships were identified there.

Melnikov method is an analytical tool to study chaos. It has been used to investigate chaos of numerous dynamic models, such as the suspend elastic cable under combined parametrical and external excitations (Zhang and Tang, 2002), a parametrically excited cantilever beam (Zhang et al., 2005), a rotor-active magnetic bearing system with time-varying stiffness (Zhang et al., 2006), a string-beam coupled system with two-degrees-of-freedom (Zhang and Cao, 2006), a cantilever beam subjected to a harmonic axial excitation and two transverse excitations at the free end (Zhang et al., 2009b), a composite laminated piezoelectric rectangular plate (Zhang et al., 2009a), a parametrically excited viscoelastic moving belt (Yao et al., 2012), and a laminated composite

* Corresponding author.
E-mail address: zlqrex@sina.com (L. Zhou).

https://doi.org/10.1016/j.oceaneng.2019.106729
Received 22 July 2019; Received in revised form 11 October 2019; Accepted 10 November 2019
Available online 25 November 2019

piezoelectric rectangular plate (Yao and Zhang, 2014), et al. Recently, some researchers have also used this method to investigate chaotic motions in ship models. With extended Melnikov's method, Wu and Mccue (2008) studied single-degree-of-freedom vessel roll motion of ships. Two roll motion models, that is a simple roll model with nonlinear damping and cubic restoring moment and the model with biased restoring moment, were analyzed there. Using the Melnikov method and numerical methods, Maki et al. (2010, 2014) investigated chaos of ship roll equation in beam seas. Chaos threshold was presented. With random Melnikov method and phase space flux, Tang et al. (2004) studied nonlinear roll and capsize of ships in the random seas. It was shown that phase space flux was growing continually along with significant wave height and the safe basin of ships was decreasing rapidly. Liu et al. (2016) analyzed stability and capsizing of nonlinear ship rolling in wind and stochastic beam seas by using random Melnikov function and the concept of phase space flux. Based on stochastic Melnikov function and phase space transport theory, Zhang et al. (2017) studied safety degree of ship capsizing in stochastic waves.

In this paper, chaotic motions for the parametrically excited roll motion of a ship in regular longitudinal waves are studied both analytically and numerically. System parameter conditions for chaos arising from homoclinic and heteroclinic intersections are presented rigorously. Chaotic feature on system parameters is investigated in detail. The results show that the critical values of chaos for homoclinic orbits increase monotonously as the increasing of the nonlinear roll attenuation coefficient, while the critical values of chaos for heteroclinic cycle decrease monotonously as the increasing of the nonlinear roll attenuation coefficient. Meanwhile, critical values of chaos for both homoclinic orbits and heteroclinic cycle increase monotonously as the increasing of the excitation amplitude. Another interesting finding is that chaotic bands may exist in this system. With the fourth-order Runge–Kutta method and the wolf algorithm, the phase portraits, time history curves, Poincaré section and Lyapunov exponent spectrum are obtained, respectively, which confirm the analytical results.

2. The mathematical model and problem formulation

The nonlinear dynamic model for parametric rolling system of ship in regular longitudinal waves is (Sanchez and Nayfeh, 1990)

$$\ddot{\varphi} + \mu_1\dot{\varphi} + \mu_3\dot{\varphi}^3 + \omega_0^2[\varphi + \alpha_3\varphi^3 + \alpha_5\varphi^5 + h_0\varphi\cos(\omega t)] = 0 \tag{1}$$

where φ is the roll angle, h_0 is the dimensionless parameter excitation amplitude, ω is the parametric excitation frequency, μ_1 and μ_3 are roll attenuation coefficients, α_3 and α_5 are dimensionless restoring moment coefficients, and ω_0 is the natural frequency of ship rolling, respectively.

Denoting $A = \omega_0^2$, $B = \omega_0^2\alpha_3$, $C = \omega_0^2\alpha_5$ and $f = \omega_0^2 h_0$, system (1) can be written as

$$\ddot{\varphi} + \mu_1\dot{\varphi} + \mu_3\dot{\varphi}^3 + A\varphi + B\varphi^3 + C\varphi^5 + f\varphi\cos(\omega t) = 0 \tag{2}$$

Assuming the roll attenuation coefficients and excitation amplitude are small, denoting $\mu_1 = \varepsilon\bar{\mu}_1$, $\mu_3 = \varepsilon\bar{\mu}_3$ and $f = \varepsilon\bar{f}$, system (2) can be written as follows

$$\ddot{\varphi} + \varepsilon\bar{\mu}_1\dot{\varphi} + \varepsilon\bar{\mu}_3\dot{\varphi}^3 + A\varphi + B\varphi^3 + C\varphi^5 + \varepsilon\bar{f}\varphi\cos(\omega t) = 0 \tag{3}$$

When $\varepsilon = 0$, the unperturbed system of (3) is

$$\ddot{\varphi} + A\varphi + B\varphi^3 + C\varphi^5 = 0 \tag{4}$$

According to the practical significance of parameters, we consider the case of $A > 0$, $B < 0$ and $C > 0$ with $B^2 - 4AC > 0$. In this case, there are five equilibrium points for the unperturbed Eq. (4), given by

$$-\varphi_2, -\varphi_1, 0, \varphi_1 = \sqrt{\frac{-B-\sqrt{B^2-4AC}}{2C}}, \varphi_2 = \sqrt{\frac{-B+\sqrt{B^2-4AC}}{2C}} \tag{5}$$

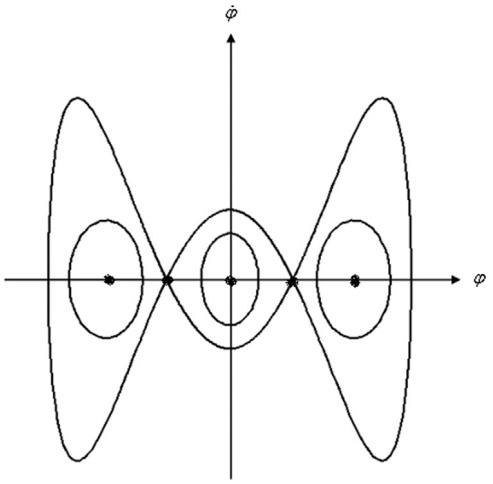

Fig. 1. The phase portrait of the unperturbed system (4).

where $0 < \varphi_1 < \varphi_2$ are well-defined quantities. Eq. (3) can be rewritten as

$$\ddot{\varphi} + \varepsilon\bar{\mu}_1\dot{\varphi} + \varepsilon\bar{\mu}_3\dot{\varphi}^3 + C\varphi(\varphi^2-\varphi_1^2)(\varphi^2-\varphi_2^2) + \varepsilon\bar{f}\varphi\cos(\omega t) = 0 \tag{6}$$

Putting the parameters

$$\theta = \frac{\varphi_2}{\varphi_1} = \sqrt{\frac{-B+\sqrt{B^2-4AC}}{-B-\sqrt{B^2-4AC}}}, \gamma = \varphi_1^2\sqrt{2C(\theta^2-1)}, \beta = \frac{5-3\theta^2}{3\theta^2-1} \tag{7}$$

the homoclinic orbits and heteroclinic cycle of the saddle φ_1 can be described as follows

$$\begin{cases} \varphi_{\text{hom}}(t) = \pm\sqrt{2}\varphi_1\frac{\cosh(\gamma t/2)}{\sqrt{\beta+\cosh(\gamma t)}} \\ \dot{\varphi}_{\text{hom}}(t) = \pm\frac{\sqrt{2}}{2}\varphi_1\gamma(\beta-1)\frac{\sinh(\gamma t/2)}{(\beta+\cosh(\gamma t))^{3/2}} \end{cases} \tag{8}$$

$$\begin{cases} \varphi_{\text{het}}(t) = \pm\sqrt{2}\varphi_1\frac{\sinh(\gamma t/2)}{\sqrt{-\beta+\cosh(\gamma t)}} \\ \dot{\varphi}_{\text{het}}(t) = \pm\frac{\sqrt{2}}{2}\varphi_1\gamma(1-\beta)\frac{\cosh(\gamma t/2)}{(-\beta+\cosh(\gamma t))^{3/2}} \end{cases} \tag{9}$$

The phase portrait of the unperturbed system (4) is shown as in Fig. 1.

3. Chaos of the system

In this section, we use the Melnikov method (Wiggins, 1990; Guckenheimer and Holmes, 1997; Li and Chen, 2012) to investigate the chaotic motions arising from the transverse intersections of stable and unstable manifolds for the homoclinic orbits and heteroclinic cycle in system (3).

3.1. Melnikov functions and parameter conditions of chaos for the system

Computing the Melnikov function of system (3) along the homoclinic orbit (8), one can obtain that

$$\begin{aligned} M_{\text{hom}}(t_0) &= -\bar{\mu}_1\int_{-\infty}^{+\infty}[\dot{\varphi}_{\text{hom}}(t)]^2\mathrm{d}t - \bar{\mu}_3\int_{-\infty}^{+\infty}[\dot{\varphi}_{\text{hom}}(t)]^4\mathrm{d}t \\ &\quad - \bar{f}\int_{-\infty}^{+\infty}\varphi_{\text{hom}}(t)\dot{\varphi}_{\text{hom}}(t)\cos(\omega(t+t_0))\mathrm{d}t \\ &= -\bar{\mu}_1\int_{-\infty}^{+\infty}[\dot{\varphi}_{\text{hom}}(t)]^2\mathrm{d}t - \bar{\mu}_3\int_{-\infty}^{+\infty}[\dot{\varphi}_{\text{hom}}(t)]^4\mathrm{d}t \\ &\quad + \bar{f}\sin\omega t_0\int_{-\infty}^{+\infty}\varphi_{\text{hom}}(t)\dot{\varphi}_{\text{hom}}(t)\sin\omega t\mathrm{d}t \\ &\equiv -\bar{\mu}_1 I_1 - \bar{\mu}_3 I_2 + \bar{f} I_3\sin\omega t_0 \end{aligned} \tag{10}$$

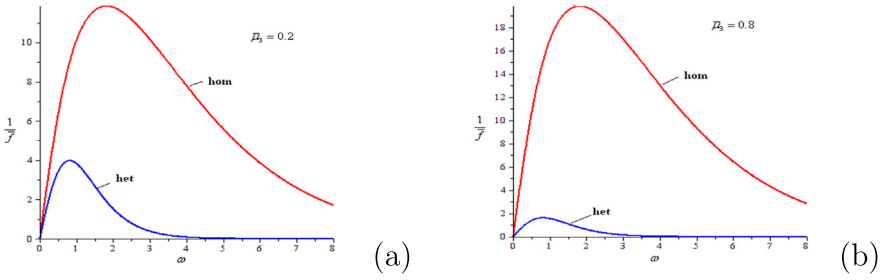

Fig. 2. The critical curves of chaos for (a) $\bar{\mu}_3 = 0.2$, (b) $\bar{\mu}_3 = 0.8$.

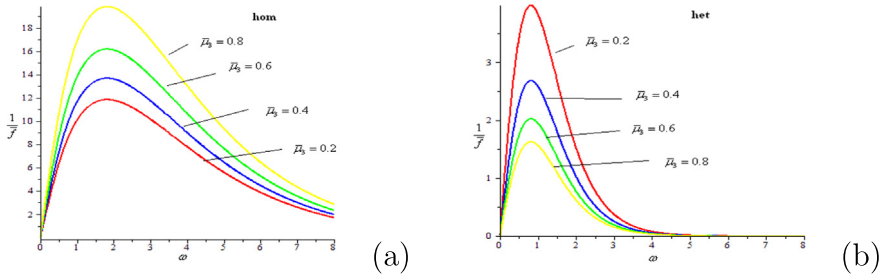

Fig. 3. The critical curves of chaos for the (a) homoclinic orbits and (b) heteroclinic cycle with different values of $\bar{\mu}_3$.

where

$$\begin{aligned}
I_1 &= \int_{-\infty}^{+\infty} [\dot{\varphi}_{\text{hom}}(t)]^2 \mathrm{d}t \\
&= \frac{\varphi_1^2 \gamma}{1+\beta}\left[-\frac{1+2\beta}{2\sqrt{1-\beta^2}} \arctan\sqrt{\frac{1-\beta}{1+\beta}} + \frac{2+\beta}{4}\right], \\
I_2 &= \int_{-\infty}^{+\infty} [\dot{\varphi}_{\text{hom}}(t)]^4 \mathrm{d}t \\
&= \frac{\varphi_1^4 \gamma^3}{320(1+\beta)^2(1-\beta)^3}\sqrt{\frac{1+\beta}{1-\beta}} \\
&\times \left[\sqrt{\frac{1-\beta}{1+\beta}}(2\beta^5 - 18\beta^4 - 139\beta^3 - 249\beta^2 - 178\beta - 48)\right. \\
&+ \left.\arctan\sqrt{\frac{1-\beta}{1+\beta}}(120\beta^3 + 240\beta^2 + 210\beta + 60)\right], \\
I_3 &= \int_{-\infty}^{+\infty} \varphi_{\text{hom}}(t)\dot{\varphi}_{\text{hom}}(t)\sin(\omega t)\mathrm{d}t \\
&= \pi\varphi_1^2\sqrt{\frac{1-\beta}{1+\beta}}\frac{\omega}{\gamma}\frac{\sinh(\omega \arccos\beta/\gamma)}{\sinh(\omega\pi/\gamma)},
\end{aligned} \tag{11}$$

Thus, $M_{\text{hom}}(t_0)$ has simple zeros and chaotic motions occur if and only if

$$\left|\frac{\bar{\mu}_1 I_1 + \bar{\mu}_3 I_2}{\bar{f} I_3}\right| < 1 \tag{12}$$

Similarly, the Melnikov function for the system (3) along the heteroclinic cycle (9) is as follows:

$$\begin{aligned}
M_{\text{het}}(t_0) &= -\bar{\mu}_1 \int_{-\infty}^{+\infty} [\dot{\varphi}_{\text{het}}(t)]^2 \mathrm{d}t - \bar{\mu}_3 \int_{-\infty}^{+\infty} [\dot{\varphi}_{\text{het}}(t)]^4 \mathrm{d}t \\
&- \bar{f} \int_{-\infty}^{+\infty} \varphi_{\text{het}}(t)\dot{\varphi}_{\text{het}}(t)\cos(\omega(t+t_0))\mathrm{d}t \\
&= -\bar{\mu}_1 \int_{-\infty}^{+\infty} [\dot{\varphi}_{\text{het}}(t)]^2 \mathrm{d}t - \bar{\mu}_3 \int_{-\infty}^{+\infty} [\dot{\varphi}_{\text{het}}(t)]^4 \mathrm{d}t \\
&+ \bar{f}\sin\omega t_0 \int_{-\infty}^{+\infty} \varphi_{\text{het}}(t)\dot{\varphi}_{\text{het}}(t)\sin\omega t \mathrm{d}t \\
&\equiv -\bar{\mu}_1 J_1 - \bar{\mu}_3 J_2 + \bar{f} J_3 \sin\omega t_0
\end{aligned} \tag{13}$$

where

$$\begin{aligned}
J_1 &= \int_{-\infty}^{+\infty} [\dot{\varphi}_{\text{het}}(t)]^2 \mathrm{d}t \\
&= \frac{\varphi_1^2 \gamma}{1+\beta}\left[\frac{1+2\beta}{2\sqrt{1-\beta^2}} \arctan\sqrt{\frac{1+\beta}{1-\beta}} + \frac{2+\beta}{4}\right], \\
J_2 &= \int_{-\infty}^{+\infty} [\dot{\varphi}_{\text{het}}(t)]^4 \mathrm{d}t \\
&= \frac{\varphi_1^4 \gamma^3}{320(1+\beta)^3(1-\beta)^2}\sqrt{\frac{1-\beta}{1+\beta}} \\
&\times \left[\sqrt{\frac{1+\beta}{1-\beta}}(2\beta^5 - 22\beta^4 - 99\beta^3 - 11\beta^2 + 82\beta + 48)\right. \\
&+ \left.\arctan\sqrt{\frac{1+\beta}{1-\beta}}(120\beta^3 + 240\beta^2 + 210\beta + 60)\right], \\
J_3 &= \int_{-\infty}^{+\infty} \varphi_{\text{het}}(t)\dot{\varphi}_{\text{het}}(t)\sin(\omega t)\mathrm{d}t \\
&= \pi\varphi_1^2\sqrt{\frac{1-\beta}{1+\beta}}\frac{\omega}{\gamma}\frac{\sinh(\omega \arccos(-\beta)/\gamma)}{\sinh(\omega\pi/\gamma)},
\end{aligned} \tag{14}$$

Therefore, $M_{\text{het}}(t_0)$ has simple zeros and chaotic motions occur if and only if

$$\left|\frac{\bar{\mu}_1 J_1 + \bar{\mu}_3 J_2}{\bar{f} J_3}\right| < 1 \tag{15}$$

3.2. Chaotic feature on the system parameters

The chaotic feature on the system parameters will be discussed in this subsection. We take $\omega_0 = 1$, $\alpha_3 = -0.8046$ and $\alpha_5 = 0.081$ in the flowing discussions. Consequently, there are three system parameters μ_1, μ_3 and f which may lead to chaos. We will fix two of them and discuss the other one in the following discussions.

Case 1: $\bar{\mu}_1$ and $\bar{\mu}_3$ are fixed

In this case, the conditions of chaotic motions are as follows, respectively,

For the homoclinic orbits:

$$\frac{1}{\bar{f}} < \left|\frac{I_3}{\bar{\mu}_1 I_1 + \bar{\mu}_3 I_2}\right| \tag{16}$$

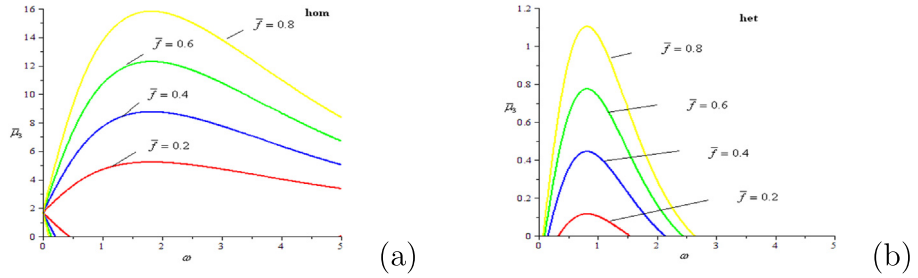

Fig. 4. The critical curves of chaos for the (a) homoclinic orbits and (b) heteroclinic cycle with different values of $\bar{f}$.

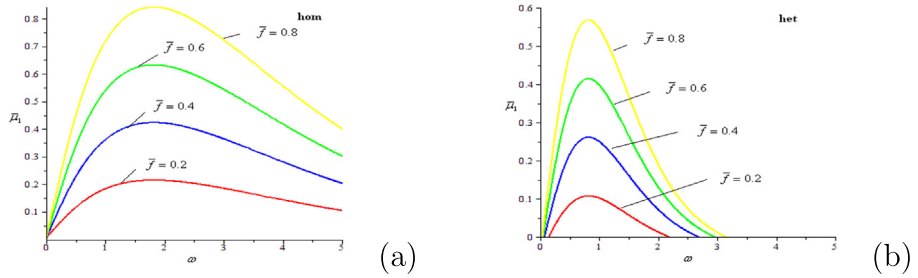

Fig. 5. The critical curves of chaos for the (a) homoclinic orbits and (b) heteroclinic cycle with different values of $\bar{\mu}_1$.

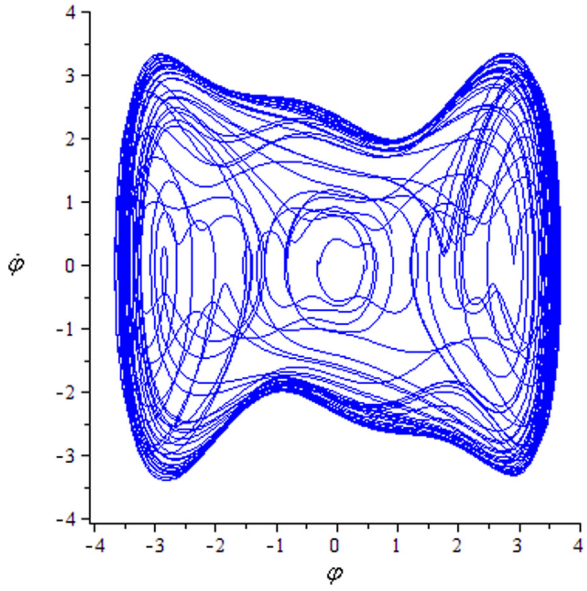

Fig. 6. The phase portraits of system (1) while $h_0 = 1.2$.

For the heteroclinic cycle:

$$\frac{1}{\bar{f}} < |\frac{J_3}{\bar{\mu}_1 J_1 + \bar{\mu}_3 J_2}| \tag{17}$$

Taking $\bar{\mu}_1 = 0.1$, $\bar{\mu}_3 = 0.2$ or $\bar{\mu}_3 = 0.8$, the critical curves of chaos are shown as in Fig. 2, from which one can see that the critical values of the heteroclinic cycle are always below that of the homoclinic orbits. This means that the heteroclinic cycle is easier chaotically excited than homoclinic orbits.

Fixing $\bar{\mu}_1 = 0.1$, taking $\bar{\mu}_3 = 0.2, 0.4, 0.6, 0.8$, the critical curves of chaos for the homoclinic orbits and heteroclinic cycle are shown as in Fig. 3, from which one can obtain that the critical values of chaos for homoclinic orbits increase monotonously as the increasing of $\bar{\mu}_3$, while the critical values of chaos for heteroclinic cycle decrease monotonously as the increasing of $\bar{\mu}_3$.

Case 2: $\bar{\mu}_1$ and $\bar{f}$ are fixed

In this case, the conditions of chaotic motions are as follows, respectively.

For the homoclinic orbits:

$$|\bar{\mu}_1 I_1 + \bar{\mu}_3 I_2| < |\bar{f} I_3| \tag{18}$$

It can be verified that $I_1 > 0$, $I_2 < 0$ and $I_3 > 0$ for all $\omega > 0$. On the other hand, the parameters $\bar{\mu}_1$, $\bar{\mu}_3$ and $\bar{f}$ are all positive, so the condition (20) can be written as follows

$$\max(0, \frac{\bar{f} I_3 - \bar{\mu}_1 I_1}{I_2}) < \bar{\mu}_3 < -\frac{\bar{f} I_3 + \bar{\mu}_1 I_1}{I_2} \tag{19}$$

For the heteroclinic cycle:

$$|\bar{\mu}_1 J_1 + \bar{\mu}_3 J_2| < |\bar{f} J_3| \tag{20}$$

Since $J_1 > 0$, $J_2 < 0$ and $J_3 > 0$ for all $\omega > 0$, condition (22) can be written as

$$\bar{\mu}_3 < \frac{\bar{f} J_3 - \bar{\mu}_1 J_1}{J_2} (\bar{f} J_3 - \bar{\mu}_1 J_1 > 0) \tag{21}$$

Fixing $\bar{\mu}_1 = 0.1$, taking $\bar{f}_3 = 0.2, 0.4, 0.6, 0.8$, respectively, the critical curves of chaos for the homoclinic orbits and heteroclinic cycle are shown as in Fig. 4, from which one can see that there exist "chaotic bands" for homoclinic orbits when the excitation frequency is small. The excitation frequency range of the chaotic band decreases monotonously as the increasing of $\bar{f}$, while the width of the chaotic band increases as the increasing of $\bar{f}$. One can also see that the heteroclinic cycle can be chaotically excited only in a interval of the excitation frequency, and the interval increases as the increasing of the excitation amplitude.

Case 3: $\bar{\mu}_3$ and $\bar{f}$ are fixed

In this case, due to $I_1 > 0$, $I_2 < 0$, $I_3 > 0$, $J_1 > 0$, $J_2 < 0$ and $J_3 > 0$ for all $\omega > 0$, the conditions of chaotic motions are as follows, respectively,

For the homoclinic orbits:

$$\max(0, \frac{-\bar{f} I_3 - \bar{\mu}_3 I_2}{I_1}) < \bar{\mu}_1 < \frac{\bar{f} I_3 - \bar{\mu}_3 I_2}{I_1} \tag{22}$$

For the heteroclinic cycle:

$$\bar{\mu}_1 < \frac{\bar{f} J_3 - \bar{\mu}_3 J_2}{J_1} (\bar{f} J_3 - \bar{\mu}_3 J_2 > 0) \tag{23}$$

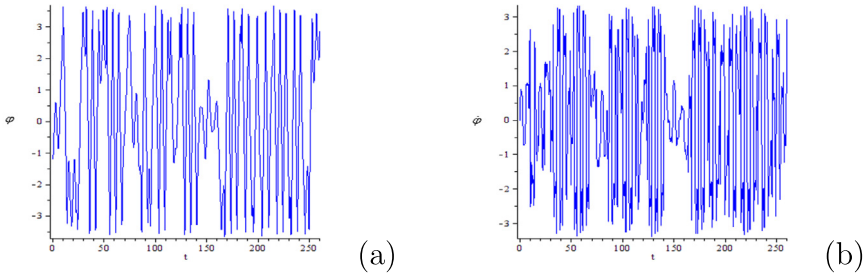

Fig. 7. The time history curves of (a) φ, (b) $\dot{\varphi}$ for system (1) while $h_0 = 1.2$.

Fixing $\bar{\mu}_3 = 0.1$, taking $\bar{f}_3 = 0.2, 0.4, 0.6, 0.8$, respectively, one can verify that $\bar{f} I_3 - \bar{\mu}_3 I_2 < 0$ for all $\omega > 0$, so condition (24) can be written as

$$\bar{\mu}_1 < \frac{\bar{f} I_3 - \bar{\mu}_3 I_2}{I_1} \tag{24}$$

The critical curves of chaos for the homoclinic orbits and heteroclinic cycle are shown as in Fig. 5. It can be concluded that the critical values of chaos for both homoclinic orbits and heteroclinic cycle increase monotonously as the increasing of the excitation amplitude. Similarly as case 2, the heteroclinic cycle can be chaotically excited only in a interval of the excitation frequency, and the interval increases as the increasing of the excitation amplitude.

4. Numerical simulations

In this section, taking a maritime patrol ship for example, numerical simulations are given to verify the analytical results.

Choosing the parameters as follows: the length of the ship is 49 m, the width is 7.4 m, the full load draft is 2.317 m, the full load displacement is 241.14t, the initial metacentric height is 0.987 m, the initial natural frequency of rolling is 1.118rad/s, the total mass moment of inertia is $268.42\mathrm{t}\cdot\mathrm{m}$, then the parameters in system (1) are $\omega = 2.236$, $\omega_0 = 1.118$, $\mu_1 = \varepsilon\bar{\mu}_1 = 0.069$, $\mu_3 = \varepsilon\bar{\mu}_3 = 0.08$, $\alpha_3 = -0.8046$, $\alpha_5 = 0.081$, $h_0 = 1.2$, respectively. Using the fourth-order Runge–Kutta method, the phase portraits and time history curves are shown as in Figs. 6–7, respectively. The Poincaré section is shown as in Fig. 8. Using the wolf algorithm (Wolf et al., 1985), the Lyapunov exponent spectrum is shown as in Fig. 9. The largest Lyapunov exponent is $0.5467 > 0$, so the system undergoes chaotic motions. On the other hand, one can compute that $|\frac{\bar{\mu}_1 I_1 + \bar{\mu}_3 I_2}{\bar{f} I_3}| = 0.1453 < 1$ and $|\frac{\bar{\mu}_1 J_1 + \bar{\mu}_3 J_2}{\bar{f} J_3}| = 0.2909 < 1$, i.e., conditions (12) and (15) are satisfied, so the system is chaotically excited according the analytical method, which agrees with the numerical results.

Lastly, choosing $h_0 = 1.1, 1.15, 1.25, 1.3$, respectively, one can obtain the phase portraits shown as in Figs. 10–13. From Figs. 10–13 and 6, it can be seen that as the increasing of the excitation amplitude, first the system undergoes periodic motions, then chaotic motions occur; at last it undergoes periodic motions again.

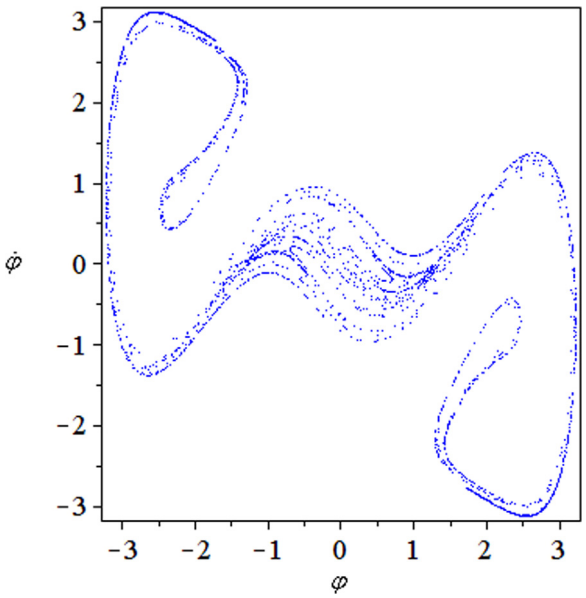

Fig. 8. The Poincaré sections of system (1) while $h_0 = 1.2$.

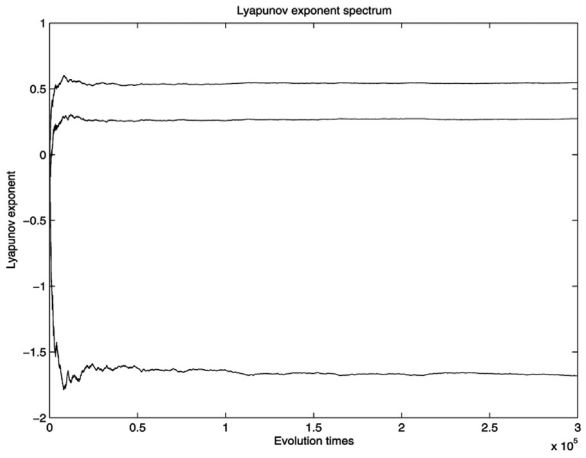

Fig. 9. The Lyapunov exponent spectrum of system (1) for $h_0 = 1.2$.

5. Conclusions

With the Melnikov method and numerical methods, chaotic dynamics for the parametrically excited roll motion of a ship in regular longitudinal waves is investigated in this paper. The critical curves separating the chaotic and non-chaotic regions are plotted. It is presented that the critical values of chaos for homoclinic orbits increase monotonously as the increasing of the nonlinear roll attenuation coefficient, while the critical values of chaos for heteroclinic cycle decrease monotonously as the increasing of the nonlinear roll attenuation coefficient. Nevertheless, the critical values of chaos for both homoclinic orbits and heteroclinic cycle increase monotonously as the increasing of the excitation amplitude. It is also demonstrated that there exist chaotic bands for this model, and the excitation frequency range of the chaotic band decreases monotonously as the increasing of the excitation amplitude, while the width of the chaotic band increases as the increasing of the excitation amplitude. The results provide some inspiration and guidance for the analysis and dynamics design of ships, for example, we should choose the system parameters suitably so that they are not in the chaotic regions. Otherwise, chaotic motion occurs and capsize may happen.

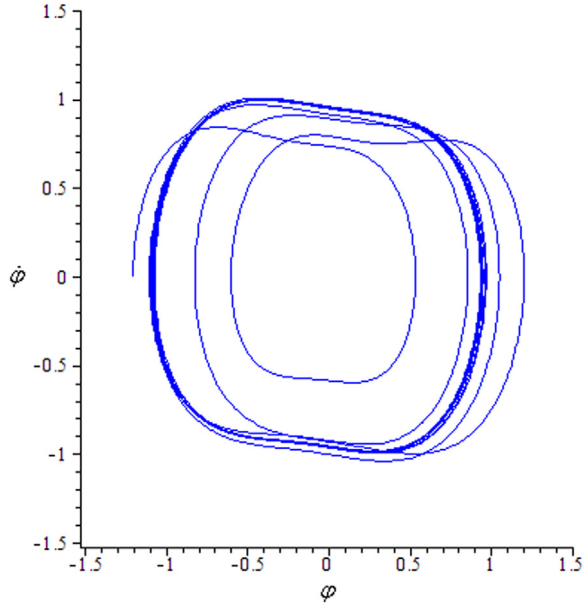

Fig. 10. The phase portraits of system (1) while $h_0 = 1.1$.

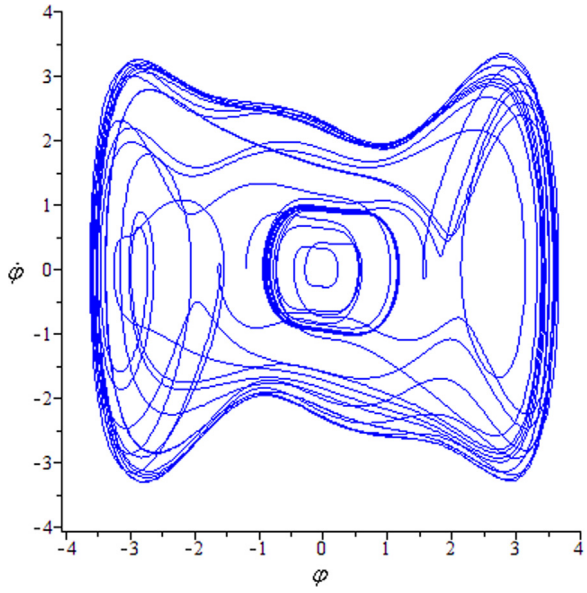

Fig. 11. The phase portraits of system (1) while $h_0 = 1.15$.

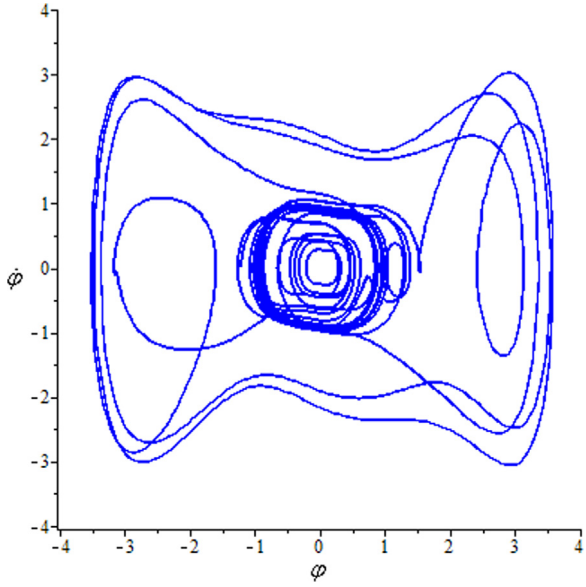

Fig. 12. The phase portraits of system (1) while $h_0 = 1.25$.

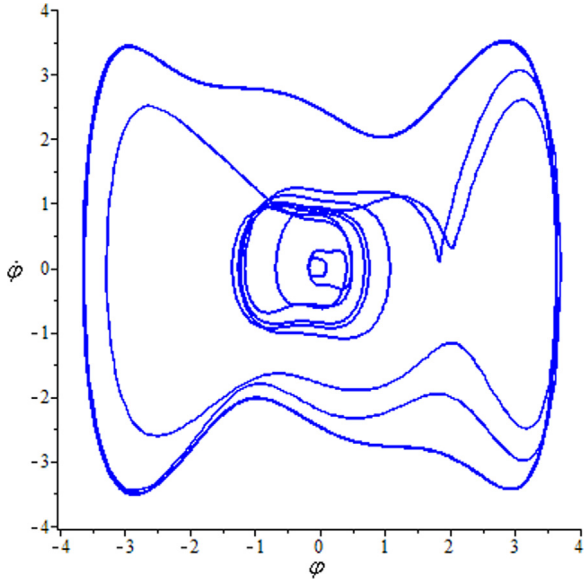

Fig. 13. The phase portraits of system (1) while $h_0 = 1.3$.

Declaration of competing interest

The authors declare that they have no known competing financial interests or personal relationships that could have appeared to influence the work reported in this paper.

Acknowledgments

The research is supported by National Natural Science Foundation of China (Nos. 11772148, 11572148, 11872201), and China Postdoctoral Science Foundation (No. 2013T60531).

References

Falzarano, J.M., Shaw, S.W., Troesch, A.W., 1992. Application of global methods for analyzing dynamical systems to ship rolling motion and capsizing. Int. J. Bifurcation Chaos 2, 101–115.

Guckenheimer, J., Holmes, P., 1997. Nonlinear Oscillations, Dynamical Systems and Bifurcations of Vector Fields. Sprigner-Verlag, New York.

Hu, K.Y., Ding, Y., Wang, H.W., 2010. Chaotic roll motions of ships in regular longitudinal waves. J. Mar. Sci. Appl. 9, 208–212.

Kan, M., Taguchi, H., 1990. Capsizing of a ship in quartering seas (part 2-chaos and fractal in capsizing phenomenon). J. Japan Soc. Nav. Arch. Ocean Eng. 168, 211–220 (in Japanese).

Kan, M., Taguchi, H., 1991. Capsizing of a ship in quartering seas (part 3-chaos and fractal in asymmetric capsizing equation). J. Japan Soc. Nav. Arch. Ocean Eng. 169, 1–13 (in Japanese).

Kan, M., Taguchi, H., 1992. Capsizing of a ship in quartering seas (Part 4. Chaos and fractals in forced mathieu type capsize equation). J. Japan Soc. Nav. Arch. Ocean Eng. 173, 83–98 (in Japanese).

Li, J.B., Chen, F.J., 2012. Chaos, Melnikov Method and Its New Development, second ed. Science Press, Beijing.

Li, M.W., Geng, J., Han, D.F., Zheng, T.J., 2016. Ship motion prediction using dynamic seasonal RvSVR with phase space reconstruction and the chaos adaptive efficient FOA. Neurocomputing 174, 661–680.

Liu, Y.C., Han, F.L., Lu, Y., 2016. Stability and capsizing analysis of nonlinear ship rolling in wind and stochastic beam seas. Appl. Ocean Res. 57, 52–63.

Liu, L.Q., Tang, Y.G., 2013. The random jumping of ship rolling in narrowband wave considering the static effect of liquid on board. J. Vib. Control 19, 576–584.

Liu, S., Yang, Z., 2011. Real-time online forecasting model of ship rolling motion based on chaotic online LSSVM. In: 2011 IEEE 18th International Conference on Industrial Engineering and Engineering Management, vol. 3, pp. 1732–1736.

Maki, A., Umeda, N., Ueta, T., 2010. Melnikov integral formula for beam sea roll motion utilizing a non-hamiltonian exact heteroclinic orbit. J. Mar. Sci. Technol. 15, 102–106.

Maki, A., Umeda, N., Ueta, T., 2014. Melnikov integral formula for beam sea roll motion utilizing a non-hamiltonian exact heteroclinic orbit: analytic extension and numerical validation. J. Mar. Sci. Technol. 19, 257–264.

Nayfeh, A.H., Sanchez, N.E., 1986. Chaos and dynamic instability in the rolling motion of ships. In: 17th Symposium on Naval Hydrodynamics, pp. 617–630.

Sanchez, N.E., Nayfeh, A.H., 1990. Nonlinear rolling motions of ships in longitudinal waves. Int. Shipbuild. Prog. 37, 247–272.

Tang, Y.G., Gu, J.Y., Zheng, H.Y., Li, H.X., 2004. Study on the ship capsize in random beam seas using melnikov method. J. Ship Mech. 8, 27–34 (in Chinese).

Virgin, L.N., 1987. The nonlinear rolling response of a vessel including chaotic motions leading to capsize in regular seas. Appl. Ocean Res. 9, 89–95.

Wiggins, S., 1990. Introduction To Applied Non-Linear Dynamical Systems and Chaos. Springer, New York.

Wolf, A., Swift, J.B., Swinney, H.L., Vastano, J.A., 1985. Determining Lyapunov exponents from a time series. Physica D 16, 285–317.

Wu, W., Mccue, L., 2008. Application of the extended Melnikov's method for single-degree-of-freedom vessel roll motion. Ocean Eng. 35, 1739–1746.

Yao, M.H., Zhang, W., 2014. Multi-pulse chaotic motions of high-dimension nonlinear system for a laminated composite piezoelectric rectangular plate. Meccanica 49, 365–392.

Yao, M.H., Zhang, W., Jean, W., 2012. Multi-pulse chaotic dynamics in non-planar motion of parametrically excited viscoelastic moving belt. J. Sound Vib. 331, 2624–2653.

Zhang, W., Cao, D.X., 2006. Studies on bifurcation and chaos of a string-beam coupled system with two-degrees-of-freedom. Nonlinear Dynam. 45, 131–147.

Zhang, W., Gao, M.J., Yao, M.H., Yao, Z.G., 2009a. Higher-dimensional chaotic dynamics of a composite laminated piezoelectric rectangular plate. Sci. China Ser. G 52, 1989–2000.

Zhang, W., Tang, Y., 2002. Global dynamics of the cable under combined parametrical and external excitations. Int. J. Non-Linear Mech. 37, 505–526.

Zhang, J.W., Wang, W.Q., Hu, J.Q., 2017. Study on the safety degree of ship capsizing in stochastic waves. J. Ship Prod. Des. 33, 24–30.

Zhang, W., Wang, F.X., Yao, M.H., 2005. Global bifurcations and chaotic dynamics in nonlinear nonplanar oscillations of a parametrically excited cantilever beam. Nonlinear Dynam. 40, 251–279.

Zhang, W., Yao, M.H., Zhan, X.P., 2006. Multi-pulse chaotic motions of a rotor-active magnetic bearing system with time-varying stiffness. Chaos Solitons Fractals 27, 175–186.

Zhang, W., Yao, M.H., Zhang, J.H., 2009b. Using the extended Melnikov method to study the multi-pulse global bifurcations and chaos of a cantilever beam. J. Sound Vib. 319, 541–569.